The Astrophysical Journal, 868:120 (13pp), 2018 December 1 https://doi.org/10.3847/1538-4357/aaeb91

The Mediation of Collisionless Oblique Magnetized Shocks by Energetic Particles

P. Mostafavi[1,2], G. P. Zank[1,3], and G. M. Webb[3]
[1] Department of Space Science, University of Alabama in Huntsville, Huntsville, AL 35899, USA
[2] Department of Astrophysical Sciences, Princeton University, Princeton, NJ 08544, USA
[3] Center for Space Plasma and Aeronomic Research (CSPAR), University of Alabama in Huntsville, Huntsville, AL 35899, USA
Received 2018 September 1; accepted 2018 October 22; published 2018 November 30

Abstract

Numerous spacecraft observations reveal that many heliospheric shocks are significantly affected by the presence of energetic particles such as solar energetic particles, pickup ions (PUIs), and anomalous cosmic rays. Examples include recent observations by the *New Horizon* spacecraft that show that the PUI pressure is larger than the thermal solar wind pressure in the solar wind. *Voyager 2* observations of the heliospheric termination shock (HTS) show that it is completely mediated by suprathermal PUIs, and that the dissipation process at the HTS is not due to the thermal solar wind protons but to PUIs. We introduce a plasma model to study the structure of collisionless oblique magnetized shocks mediated by suprathermal energetic particles. We show that the incorporation of both collisionless heat flux and viscosity associated with energetic particles can completely determine the structure of collisionless oblique shocks for all angles except $\theta = 54.^{\circ}7$. The limitation at this angle is technical and comes in part from the assumed simplified form of the viscosity coefficient. In modeling the HTS, we show that PUIs are heated much more than the thermal gas through the HTS transition, and thus the HTS is mediated by PUIs. We study different values of the HTS obliquity and find that a parallel HTS heats PUIs more compared to the background thermal gas than it does at a perpendicular HTS.

Key words: magnetohydrodynamics (MHD) – shock waves – Sun: heliosphere

1. Introduction

Energetic particles are key to understanding many fundamental space plasma physics and astrophysical problems. They play a central role in physical problems such as the acceleration and propagation of galactic cosmic rays in the interstellar and interplanetary medium and shock wave structure. Energetic particles in the heliosphere (such as pickup ions (PUIs), solar energetic particles (SEPs), and anomalous cosmic rays (ACRs)) play a fundamental role in the dissipative process at shock waves, and thus in determining their structure. In numerous cases in the heliosphere, the coupling of energetic or suprathermal particles and the subsequent back-reaction on the thermal plasma cannot be ignored. For example, recent observations of shocks in the inner heliosphere show that interplanetary shocks at 1 au can have a pressure that is entirely dominated by SEPs. In these interplanetary shocks, the energetic particle pressure exceeds that of the magnetic field and the background thermal solar wind plasma (Russell et al. 2013; Lario et al. 2015a, 2015b). Riley et al. (2016) showed that the propagation and structural characteristics of these shocks is different from those expected from a simple MHD shock description. A very relevant and important example of energetic particles mediating a thermal background plasma is that of suprathermal PUIs in the heliosphere and very local interstellar medium (VLISM; i.e., the region in the ISM that is mediated by heliospheric processes and that may extend to a distance of ∼75 au from the HP; see Zank 2015 and references therein for details about the definition). An interstellar PUI in the heliosphere is created when an interstellar neutral atom enters the heliosphere and charge exchanges with a solar wind ion or is photoionized. The newly created ion (i.e., the PUI) immediately responds to the motional electric field to comove with the background solar wind. The initial PUI ring-beam distribution is unstable and excites Alfvénic fluctuations that, together with pre-existing fluctuations, scatter the PUIs to near-isotropy. The pickup and acceleration of PUIs to comove with the bulk solar wind speed slows the bulk solar wind since energy and momentum is transferred from the solar wind bulk motion into PUI pressure. PUIs provide the dominant internal pressure in the outer heliosphere and cannot be ignored. PUIs are non-thermal energetic particles and play a critical role in determining the structure of outer heliospheric shocks. Zank et al. (2014) showed that PUIs are not equilibrated with the background plasma in the supersonic solar wind beyond 10 au, the IHS (inner heliosheath, i.e., region between the HTS and the HP), and the VLISM, and need to be treated as a separate plasma component, typically in the form of a separate equation of state.

The Solar Wind Around Pluto (SWAP) instrument on the *New Horizon* spacecraft makes observations of the solar wind and suprathermal PUIs in the outer heliosphere (McComas et al. 2008). McComas et al. (2017) presented PUI observations measured by the SWAP instrument up to a distance of 38 au and showed that PUIs dominate the internal pressure, typically being larger than the thermal solar wind and magnetic pressure. Thus, shock waves in the outer heliosphere should be mediated by suprathermal PUIs.

Voyager 2 crossed the heliospheric termination shock (HTS) at 84 au in 2007. In situ *Voyager 2* measurements indicated that the primary dissipation mechanism at the HTS is not provided by thermal gas (Richardson et al. 2008). The downstream thermal plasma temperature observed by *Voyager 2* was much less than anticipated by MHD models. The possibility that the HTS should be affected significantly by suprathermal PUIs was predicted by Zank et al. (1996). PUIs are reflected preferentially at the cross-shock electrostatic potential of the HTS and acquire almost all the dissipative heating of the bulk flow energy (Zank et al. 1996, 2010; Richardson et al. 2008). The dissipation process at the HTS is therefore due primarily to the nearly isotropically shell-distributed PUIs and not to thermal

protons. Oka et al. (2011), Yang et al. (2015), Mostafavi et al. (2017a, 2017b), and Lembège & Yang (2018) showed that the flow remains supersonic with respect to the thermal gas downstream of the HTS. However, with the inclusion of PUIs, the transition from the upstream to downstream state results in a supersonic–subsonic flow transition. The insertion of a gas subshock is not necessary for the HTS with the structure being determined completely by PUI dissipation.

Thermal and non-thermal charged particles are slowed and heated as they cross the HTS and enter the IHS. The IHS is a highly turbulent medium of compressed solar wind and magnetic field, and is thermally dominated by energetic particles such as ACRs and PUIs (Decker et al. 2015). The plasma beta (β; the ratio of thermal particle pressure to magnetic pressure) with the inclusion of the energetic particle pressure is much greater than one. The large plasma beta in the IHS suggests that shock waves in this region should be mediated by energetic particles.

Suprathermal PUIs in the VLISM are created by secondary charge exchange between hot and/or fast neutral hydrogen atoms with cold VLISM protons. The suprathermal PUI population in the VLISM increases the sound speed, which can weaken or even eliminate the bow shock and instead yields a bow wave (McComas et al. 2012; Zank et al. 2013). VLISM PUIs have a very small number density of about $5 \times 10^{-5}\,\mathrm{cm}^{-3}$ (Zirnstein et al. 2014). Mostafavi & Zank (2018) showed that PUIs are not an important dissipative mechanism for VLISM shocks. *Voyager 1* observed a very unusual broad VLISM shock that was much broader than a similar shock at 1 au (Burlaga et al. 2013). Mostafavi & Zank (2018) showed that proton–proton collisions and not wave–particle interactions determine the structure of the broad VLISM shock, being mediated only by the magnetic field and thermal gas.

Several models have been introduced to study the structure of shock waves based on a relatively simple magnetohydrodynamic (MHD) description in which all particles are treated as a single fluid (see, e.g., Marshall 1955; Coroniti 1970; Sagdeev 1979; Kennel et al. 1985, and references therein). Coroniti (1970) used a single-fluid system of equations that incorporated several collisional dissipation mechanisms (heat conduction, resistivity, and viscosity), which introduce various length scales into the shock structure. Based on Coroniti's collisional model, resistivity can always initiate a fast mode shock, thermal conduction alone is sufficient only to smooth weak shock transitions, and viscosity alone cannot provide a complete smooth fast shock transition. Consequently, inclusion of only some of the dissipation terms is not enough to yield smooth physical solutions connecting the upstream to the downstream state and a subshock is necessary. Marshall (1955) found that for a perpendicular shock propagating in a cold plasma with Mach number greater than 2.76, a subshock is necessary. This Mach number is often referred to as a critical Mach number. Therefore, for a shock exceeding the critical Mach number, resistivity alone does not produce a continuous shock profile and another dissipation mechanism is then required. Kennel et al. (1985), in an extensive review of MHD shock waves, showed that another dissipation term (viscosity) must be added to resistivity in supercritical shocks to provide the dissipation required by the shock jump conditions. In the case of a one-fluid system of equations, the dissipation is applied to all particles, and the distinction between energetic particles and thermal gas is lost. Thus, the role of energetic particles in contributing to the primary dissipation mechanism at a shock transition has not been established.

The MHD description of the HTS anticipated that the downstream thermal plasma temperature should be about 10^6 K. However, *Voyager 2* measured the core temperature of the thermal gas to be about 180,000 K, far less than the expected 10^6 K. Instead, most of the energy went into PUIs through their reflection at the quasi-perpendicular HTS front. Thus, it is necessary to distinguish thermal gas from energetic particles. In this work, we address the dissipation mechanisms introduced by energetic particles that are responsible for determining the structure of shocks in the heliosphere and possibly elsewhere.

Drury & Völk (1981) and Axford et al. (1982) used a hydrodynamic form of the so-called cosmic-ray two-fluid model to study shock wave structure. They introduced a hydrodynamic model in which energetic particles or cosmic rays were assumed to have a very small (negligible) number density but contributed to the system through their energy density and pressure. The energetic particle distribution function was assumed to be nearly isotopic and governed by a transport equation correct to the first order in anisotropy (the Parker–Gleeson–Axford transport equation). As found by Drury & Völk (1981) and Axford et al. (1982), heat conduction (or spatial diffusion) alone is sometimes insufficient to smooth the structure of all possible shocks since double-valued downstream solutions exist for a fixed upstream state. For example, when upstream energetic particles have a small pressure, the energetic particle heat conduction is insufficient to smooth the shock wave and a gas subshock should be added. Webb (1983) extended the hydrodynamic cosmic-ray two-fluid model to include a magnetic field and considered the case of oblique MHD shocks. Webb (1983) investigated the shock structure for a cold gas upstream and found that in some Mach number regimes the energetic particles' heat conduction term was not sufficient to smooth the shock transition, requiring a gas subshock to determine the downstream state. This result is quite distinct from the hydrodynamic cold gas case, which is always smoothed by energetic particles (Axford et al. 1982). Webb et al. (1986) studied the structure of MHD shock waves for a non-zero upstream thermal gas pressure in which they elucidated the role of switch-on gas subshocks in their model. Earl et al. (1988), Jokipii & Williams (1992), and Webb (1989) included a higher-order dissipation term (viscosity) to describe cosmic-ray transport. Jokipii & Williams (1992) included cosmic-ray viscosity to investigate hydrodynamic shock structure in the case of cold thermal plasma ($P_g = 0$). However, there is no need to add a viscosity term for this case, since all transitions are smooth when heat conduction is included and a subshock is always absent.

Based on the Zank et al. (2014) calculations of the equilibration of suprathermal PUIs with background thermal electrons and protons in the supersonic solar wind beyond 10 au, the IHS, and the VLISM, a multi-fluid system of equations is needed to describe a PUI-mediated plasma. Zank et al. (2014, 2016) and Zank (2016) developed a collisionless form of Chapman–Enskog expansion for a multi-component plasma comprising thermal protons, electrons, and energetic particles (such as PUIs, ACRs, and SEPs). PUIs drive

streaming instabilities and thus experience pitch-angle scattering from pre-existing and self-excited Alfvénic fluctuations. They form a nearly isotropically filled-shell distribution with particle speeds varying from nearly zero to twice the solar wind speed in the spacecraft frame. The Zank et al. (2014) model showed that PUIs introduce a collisionless heat flux and collisionless viscosity into the plasma system. Thus, the dissipation terms associated with energetic particles are due to wave/turbulence–particle interactions and not particle collisions. The structure of their model is identical to the cosmic-ray two-fluid model (Drury & Völk 1981; Axford et al. 1982), except the Zank et al. (2014) model includes the extra collisionless viscosity term associated with energetic particles, and the energetic particle mass is not ignored. Mostafavi et al. (2017a, 2017b) used the Zank et al. (2016, 2014) model to investigate the structure of shock waves in the presence of both collisionless energetic particle heat flux and viscosity for the case of a large plasma beta ($\beta \gg 1$). The incorporation of both energetic particle collisionless heat flux and viscosity is sufficient to completely determine the structure of a hydrodynamic shock in the absence of a magnetic field for all Mach numbers.

Most studies of the structure of shock waves have focused on purely parallel and perpendicular shock waves (e.g., Axford et al. 1982; Mostafavi et al. 2017b; Mostafavi & Zank 2018). However, interplanetary shocks are not usually purely perpendicular or parallel. Interplanetary shocks are typically oblique in that the upstream magnetic field is at an angle with respect to the shock normal. Shock properties can change from parallel to oblique and perpendicular. In part, the energy that is transferred to energetic particles and thermal plasma, as expressed by the compression ratio of the shock, depends on the obliquity of the shock. Shock waves are not necessary entirely laminar, and ripples may develop on their surfaces. Ripples on the surface of shock waves may be generated by instabilities due to reflected PUIs (Burgess & Scholer 2007; Yang et al. 2015; Lembège & Yang 2018). The HTS surface is undoubtedly affected by the conditions and the state of turbulence in the heliosheath. Five crossings of the HTS were detected by *Voyager 2* (Richardson et al. 2008), which has led to the interpretation that the HTS is not a laminar non-turbulent shock wave. It is therefore unlikely that the HTS is always perpendicular locally.

ACRs and termination shock particles (TSPs) are believed to be energetic PUIs that were accelerated at the HTS (Fisk et al. 1974; Stone et al. 2005). An ACR-mediated model presented by Florinski et al. (2009) showed that the precursor upstream of the HTS (with a scale size of ~0.3 au) might be due to mediation of the shock by ACRs. Ye et al. (2016) used a focused transport approach to study the TSPs and the obliquity of the HTS. *Voyager 1* detected a significant increase in the number of low-energy suprathermal ions about seven months before the HTS crossing (Cummings et al. 2003; McDonald et al. 2003). During this time, the TSP intensity increased by a factor of 1.5. Florinski et al. (2008) suggested that the observed low-energy suprathermal ion population, the TSPs, were accelerated by a highly oblique shock wave. Both an oblique HTS and a parallel HTS can reflect PUIs, and thus provide a population of upstream accelerated TSPs that eventually become ACRs. Such an oblique HTS is expected to exist in regions where the idealized spiral interplanetary magnetic field cuts through the HTS at an oblique angle. Therefore, the assumption that the HTS is exclusively perpendicular is unlikely to always be correct.

In the first part of this paper, we formulate the energetic-particle-mediated plasma model based on Zank et al. (2014). In the second part, we use the Zank et al. (2014, 2016) model to investigate the structure of steady-state oblique shock waves in the presence of a magnetic field when both the energetic particle collisionless viscosity and heat flux are included. The present work only considers the case of fast magnetosonic shock waves. We show that the incorporation of both collisionless heat flux and collisionless viscosity associated with energetic particles can smooth and determine the shock structure for all angles except $\theta = 54.^{\circ}7$. In some respects, the singular behavior at this angle is a technical rather than a physical limitation since the form of the viscous term formally goes to zero at this angle. In practice, relaxing some of the assumptions underlying the physical form of the viscous term would eliminate this singular behavior. For the present, we do not consider this additional complicating factor. We find that parallel shocks are typically broader than perpendicular shocks because of the difference between parallel and perpendicular heat conduction. We model the HTS and show that PUIs are heated much more than the thermal gas during the HTS transition, which is consistent with the *Voyager 2* observations (Richardson 2008). We consider both a parallel HTS and a perpendicular HTS and find that the PUIs and thermal gas are more heated and energized at the parallel than the perpendicular shock. We also model a quasi-parallel HTS and a quasi-perpendicular HTS to consider the case of an oblique HTS. In the last section, we summarize our results about the structure of collisionless oblique shock waves when mediated by energetic particles.

2. Model

In this section, we present a brief review of the formulation of the PUI or SEP-mediated plasma model presented by Zank et al. (2014, 2016), Zank (2016), and Mostafavi et al. (2017b). The heliosphere comprises thermal solar wind, suprathermal energetic particles such as PUIs or SEPs, and neutral atoms (beyond an ionization cavity of about 6–10 au). The charge exchange mean free path in the IHS is approximately 2500 au and greater than 200 au in the supersonic solar wind beyond 10 au (Zank 2015). Thus, the charge exchange mean free paths are very large, and we can ignore the coupling between neutral atoms and solar wind protons when studying the structure of shocks. Using appropriate parameters for the supersonic solar wind beyond 10 au, the IHS, and the VLISM, Zank et al. (2014) estimated the equilibration timescales of PUIs and thermal plasma in these regions. They showed that the PUIs are not equilibrated with the background thermal plasma. Zank et al. (2016) showed that SEPs with energies greater than 5 keV cannot equilibrate in the inner heliosphere. Therefore, energetic particles such as PUIs, SEPs, and ACRs are a distinct component in the plasma system. The plasma flow is described by a multi-component model comprising thermal solar wind ions and electrons with Maxwellian distributions, and an energetic ion component (PUIs, SEPs, or ACRs). The multi-component model is too complicated for most problems, but it can be reduced to a single-fluid-like model by making some assumptions (see details in Zank et al. 2014).

The collisionless diffusion or heat flux tensor and pressure tensor for the energetic particles may be expressed, respectively, as

$$\boldsymbol{K}_p = \begin{pmatrix} K_\parallel & 0 & 0 \\ 0 & K_\perp & 0 \\ 0 & 0 & K_\perp \end{pmatrix}, \tag{1}$$

$$\begin{aligned}(P_{ij}) &= P_p(\delta_{ij}) + \begin{pmatrix} -2 & 0 & 0 \\ 0 & 1 & 0 \\ 0 & 0 & 1 \end{pmatrix} \frac{\eta_{k\ell}}{15}\left(b_k b_l \frac{\partial U_k}{\partial x_\ell} - \frac{1}{3}\delta_{k\ell}\frac{\partial U_m}{\partial x_m}\right) \\ &\equiv P_p \boldsymbol{I} + \boldsymbol{\Pi}_p,\end{aligned} \tag{2}$$

where $\eta \simeq P_p \tau_s$ is the viscosity coefficient and τ_s is PUI-scattering timescale. P_p is the PUI scalar pressure and $\boldsymbol{\Pi}_p$ a stress tensor. The assumption is that the magnetic field is along the x-axis. $K_\parallel$ and $K_\perp$ are diffusion coefficients parallel and perpendicular to the magnetic field.

The reduced single-fluid-like model equations, together with the Maxwell equations, are given by (Zank et al. 2014, 2016)

$$\frac{\partial \rho}{\partial t} + \nabla \cdot (\rho \boldsymbol{U}) = 0, \tag{3}$$

$$\rho\left(\frac{\partial \boldsymbol{U}}{\partial t} + \boldsymbol{U}\cdot\nabla\boldsymbol{U}\right) = -\nabla(P_g + P_p) - \nabla\cdot\boldsymbol{\Pi_p} + \boldsymbol{J}\times\boldsymbol{B}, \tag{4}$$

$$\frac{\partial P_g}{\partial t} + \boldsymbol{U}\cdot\nabla P_g + \gamma_g P_g \nabla\cdot\boldsymbol{U} = 0, \tag{5}$$

$$\begin{aligned}&\frac{\partial P_p}{\partial t} + \boldsymbol{U}\cdot\nabla P_p + \gamma_p P_p \nabla\cdot\boldsymbol{U} \\ &\quad = \frac{1}{3}\nabla\cdot(\boldsymbol{K}_p\cdot\nabla P_{\rm p}) - (\gamma_p - 1)\boldsymbol{\Pi}_p\colon(\nabla\boldsymbol{U}),\end{aligned} \tag{6}$$

$$\begin{aligned}&\frac{\partial}{\partial t}\left(\frac{1}{2}\rho\boldsymbol{U}^2 + \frac{P_p}{\gamma_p - 1} + \frac{P_g}{\gamma_g - 1} + \frac{1}{2\mu_0}B^2\right) \\ &+\nabla\cdot\left(\frac{1}{2}\rho\boldsymbol{U}U^2 + \frac{\gamma_p}{\gamma_p - 1}P_p\boldsymbol{U} + \frac{\gamma_g}{\gamma_g - 1}P_g\boldsymbol{U} + \frac{1}{\mu_0}B^2\boldsymbol{U}\right. \\ &-\frac{1}{\mu_0} \\ &\left.\boldsymbol{U}\cdot\boldsymbol{BB} + \boldsymbol{\Pi}_p\cdot\boldsymbol{U} - \frac{1}{\gamma_p - 1}\frac{\boldsymbol{K}_p}{3}\cdot\nabla P_p\right) = 0.\end{aligned} \tag{7}$$

$$\begin{aligned}&\boldsymbol{E} = -\boldsymbol{U}\times\boldsymbol{B};\ \frac{\partial \boldsymbol{B}}{\partial t} = -\nabla\times\boldsymbol{E}; \\ &\mu_0\boldsymbol{J} = \nabla\times\boldsymbol{B};\ \nabla\cdot\boldsymbol{B} = 0,\end{aligned} \tag{8}$$

where μ_0 is the permeability of free space and $\boldsymbol{J}$ is the current density. $\boldsymbol{B}$ and $\boldsymbol{E}$ denote the magnetic and electric fields, P_p the PUI pressure, P_g the thermal gas (sum of electrons and protons) pressure, $\boldsymbol{U}$ the bulk flow velocity, and ρ the total density. We denote all quantities pertaining to PUIs and thermal gas with the subscripts p and g, respectively. $\gamma_{p/g}$ denotes the adiabatic index for PUIs/thermal gas. The viscosity and heat flux dissipation terms introduce distinct length scales into the system that are absent in MHD (see Mostafavi et al. 2017b). The single-fluid-like description also differs from the standard MHD model in that a separate Equation (6) for the non-equilibrated energetic particle distribution is required.

Since we need to consider an arbitrary orientation of the magnetic field, we rotate Equations (3)–(8) through an angle θ using the standard rotation matrix,

$$R = \begin{pmatrix} \cos\theta & -\sin\theta & 0 \\ \sin\theta & \cos\theta & 0 \\ 0 & 0 & 1 \end{pmatrix}, \tag{9}$$

to obtain

$$\frac{\partial \rho}{\partial t} + \nabla\cdot(\rho\boldsymbol{U}) = 0, \tag{10}$$

$$\rho\left(\frac{\partial \boldsymbol{U}}{\partial t} + \boldsymbol{U}\cdot\nabla\boldsymbol{U}\right) = -\nabla(P_g + P_p) - \nabla\cdot\boldsymbol{\Pi}'_p + \boldsymbol{J}\times\boldsymbol{B}, \tag{11}$$

$$\frac{\partial P_g}{\partial t} + \boldsymbol{U}\cdot\nabla P_g + \gamma_g P_g\nabla\cdot\boldsymbol{U} = 0, \tag{12}$$

$$\begin{aligned}&\frac{\partial P_p}{\partial t} + \boldsymbol{U}\cdot\nabla P_p + \gamma_p P_p\nabla\cdot\boldsymbol{U} \\ &\quad = \frac{1}{3}\nabla\cdot(\boldsymbol{K}'_p\cdot\nabla P_p) - (\gamma_p - 1)\boldsymbol{\Pi}'_p\colon(\nabla\boldsymbol{U}),\end{aligned} \tag{13}$$

$$\begin{aligned}&\frac{\partial}{\partial t}\left(\frac{1}{2}\rho\boldsymbol{U}^2 + \frac{P_p}{\gamma_p - 1} + \frac{P_g}{\gamma_g - 1} + \frac{1}{2\mu_0}B^2\right) \\ &+\nabla\cdot\left(\frac{1}{2}\rho\boldsymbol{U}\boldsymbol{U}^2 + \frac{\gamma_p}{\gamma_p - 1}P_p\boldsymbol{U} + \frac{\gamma_g}{\gamma_g - 1}P_g\boldsymbol{U} + \frac{1}{\mu_0}B^2\boldsymbol{U}\right. \\ &\left.-\frac{1}{\mu_0}\boldsymbol{U}\cdot\boldsymbol{BB} + \boldsymbol{\Pi}'_p\cdot\boldsymbol{U} - \frac{1}{\gamma_p - 1}\frac{\boldsymbol{K}'_p}{3}\cdot\nabla P_p\right) = 0,\end{aligned} \tag{14}$$

$$\begin{aligned}&\boldsymbol{E} = -\boldsymbol{U}\times\boldsymbol{B};\ \frac{\partial \boldsymbol{B}}{\partial t} = -\nabla\times\boldsymbol{E}; \\ &\mu_0\boldsymbol{J} = \nabla\times\boldsymbol{B};\ \nabla\cdot\boldsymbol{B} = 0,\end{aligned} \tag{15}$$

where

$$\boldsymbol{K}'_p = \begin{pmatrix} K_\parallel\cos^2\theta + K_\perp\sin^2\theta & (-K_\parallel + K_\perp)\sin\theta\cos\theta & 0 \\ (-K_\parallel + K_\perp)\sin\theta\cos\theta & K_\parallel\sin^2\theta + K_\perp\cos^2\theta & 0 \\ 0 & 0 & K_\perp \end{pmatrix}, \tag{16}$$

$$\begin{aligned}\boldsymbol{\Pi}'_p = &\begin{pmatrix} -2\cos^2\theta + \sin^2\theta & 3\sin\theta\cos\theta & 0 \\ 3\sin\theta\cos\theta & -2\sin^2\theta + \cos^2\theta & 0 \\ 0 & 0 & 1 \end{pmatrix} \\ &\times\frac{\eta_{k\ell}}{15}\left(b_k b_l\frac{\partial U_k}{\partial x_\ell} - \frac{1}{3}\delta_{k\ell}\frac{\partial U_m}{\partial x_m}\right).\end{aligned} \tag{17}$$

All of the equations are invariant with respect to the rotation except the stress tensor and the diffusion tensor, since they were initially derived for the case where $\boldsymbol{B}$ was only in the x direction.

We use a one-dimensional steady-state model, in which all physical quantities depend on the x coordinate of a Cartesian

coordinate system *XYZ*. The background plasma velocity $\boldsymbol{U} = (U_x,\ U_y,\ 0)$ and magnetic field $\boldsymbol{B} = (B_x,\ B_y,\ 0)$ are restricted to the $x-y$ plane. The shock surface is located along the y-axis, and the shock normal is directed along the x-axis. For a 1D flow, the viscosity tensor reduces to

$$\frac{\eta_{k\ell}}{15}\left(b_k b_l \frac{\partial U_k}{\partial x_\ell} - \frac{1}{3}\delta_{k\ell}\frac{\partial U_m}{\partial x_m}\right) \equiv \eta_p\left(\cos^2\theta - \frac{1}{3}\right)\frac{\partial U_x}{\partial x}. \quad (18)$$

By taking the integral of the one-dimensional steady-state model, the conservation laws for mass, momentum, and energy fluxes are

$$\rho U_x = \text{const}, \quad (19)$$

$$\rho U_x^2 + P_g + P_p + \frac{B_y^2}{2\mu_0} + \Pi'_{xx} = \text{const}, \quad (20)$$

$$\rho U_x U_y - \frac{1}{\mu_0}B_x B_y + \Pi'_{xy} = \text{const}, \quad (21)$$

$$\frac{1}{2}\rho U_x(U_x^2 + U_y^2) + \frac{1}{\mu_0}B_y(U_x B_y - U_y B_x) + \frac{\gamma_g}{\gamma_g - 1}P_g U_x + \frac{\gamma_p}{\gamma_p - 1}P_p U_x - \frac{K'_{xx}}{3}\frac{1}{\gamma_p - 1}\frac{\partial P_p}{\partial x} + U_x\Pi'_{xx} + U_y\Pi'_{yx} = \text{const}. \quad (22)$$

For a highly conducting fluid, the electric field is $\boldsymbol{E} = -\boldsymbol{U}\times\boldsymbol{B}$. Maxwell's Equation (8) shows that the electric field in the z direction is constant and yields

$$U_x B_y - U_y B_x = \text{const}. \quad (23)$$

Moreover, the magnetic field normal to the shock surface, B_x, is constant through the shock transition. The changes in plasma parameters across the shock must satisfy the Rankine–Hugoniot jump conditions. The plasma conditions far upstream and downstream of the shock are spatially uniform, and dissipation terms therefore do not affect these regions, unlike at the shock position. In this paper, we use the de Hoffmann–Teller frame except for the case of a perpendicular shock for which a shock-normal frame is used.

3. PUI- and SEP-mediated Shock Structure

The PUI-mediated plasma model derived in the previous section can be used to study the structure of collisionless shock waves. Here, we extend the paper of Webb (1983) and derive the general shock structure equation by taking into account both collisionless dissipation terms (heat flux and viscosity) associated with PUIs. The subscripts 1 and 2 denote the plasma quantities far upstream and downstream of the shock, respectively. The inverse compression ratio in the x direction, $y = U_x/U_{x1} = \rho_1/\rho$, is introduced as a quantity to study shock wave structure (Whitham 1974; Axford et al. 1982). The background thermal gas has no dissipation terms and is piecewise isentropic, and thus $P_g\rho^{-\gamma_g}$ is constant through the shock transition provided it is smooth. From Equations (19)–(23), one can obtain the magnetic field component and flow velocity components in terms of y as

$$B_y = B_{y1}\left[\frac{(1 - y_A)}{(y - y_A)} + 3\sin\theta\cos\theta\left(\frac{y_A}{y_A - y}\right) \times \frac{\text{Sch}_p}{\sqrt{y_A y_B}}\left(\cos^2\theta - \frac{1}{3}\right)\frac{\partial y}{\partial\bar{x}}\right], \quad (24)$$

$$\frac{U_y}{U_{x1}} = \frac{U_{y1}}{U_{x1}} + \sqrt{y_A y_B}\left(\frac{1 - y}{y - y_A}\right) + 3\sin\theta\cos\theta\text{Sch}_p\left(\frac{y}{y_A - y}\right)\left(\cos^2\theta - \frac{1}{3}\right)\frac{\partial y}{\partial\bar{x}}, \quad (25)$$

where

$$y_A = \frac{B_{x1}^2}{\rho_1 U_{x1}^2\mu_0};\ y_B = \frac{B_{y1}^2}{\rho_1 U_{x1}^2\mu_0}, \quad (26)$$

are squared inverse Alfvénic Mach numbers of the flow far upstream of the shock, θ is the angle between the shock normal and the magnetic field, $\bar{x}$ is x normalized to the diffusion length scale, i.e., $\bar{x} \equiv x/L$, $L \equiv (K_\parallel/U_{x1})$, and $\text{Sch}_p \equiv (\eta_p/\rho_1 K_p)$ is the Schmidt number. The PUI pressure equation yields

$$P_p = P_{p1} + P_{g1}(1 - y^{-\gamma_g}) + \rho_1 U_{x1}^2 \times\left(1 - y + \frac{y_B}{2}\left[1 - \left(\frac{1 - y_A}{y - y_A}\right)^2 - 9\sin^2\theta \times\cos^2\theta\text{Sch}_p^2 \times\frac{y_A}{y_B(y_A - y)^2}\left(\cos^2\theta - \frac{1}{3}\right)^2\left(\frac{\partial y}{\partial\bar{x}}\right)^2 + 6\sin\theta\cos\theta\text{Sch}_p \times\frac{1 - y_A}{(y - y_A)^2}\sqrt{\frac{y_A}{y_B}}\left(\cos^2\theta - \frac{1}{3}\right)\frac{\partial y}{\partial\bar{x}}\right] - \text{Sch}_p(-2\cos^2\theta + \sin^2\theta) \times\left(\cos^2\theta - \frac{1}{3}\right)\frac{\partial y}{\partial\bar{x}}\right). \quad (27)$$

After some algebra, a single second-order ordinary differential equation can be obtained for the structure of an

oblique shock,

$$\frac{(\cos^2\theta+\bar{k}\sin^2\theta)}{3(\gamma_p-1)}\left(\cos^2\theta-\frac{1}{3}\right)\times\left[-9\sin^2\theta\cos^2\theta\left(\cos^2\theta-\frac{1}{3}\right)\mathrm{Sch}_p^2\frac{y_A}{(y_A-y)^2}\frac{\partial y}{\partial\bar{x}}+3\sin\theta\cos\theta\mathrm{Sch}_p\sqrt{y_Ay_B}\frac{1-y_A}{(y-y_A)^2}-\mathrm{Sch}_p(-2\cos^2\theta+\sin^2\theta)\right]\frac{\partial^2y}{\partial\bar{x}^2}+\frac{(\cos^2\theta+\bar{k}\sin^2\theta)}{3(\gamma_p-1)}\left[-1+\frac{y^{-\gamma_g-1}}{M_{s1}^2}+\frac{y_B(1-y_A)^2}{(y-y_A)^3}-9\sin^2\theta\cos^2\theta\left(\cos^2\theta-\frac{1}{3}\right)^2\mathrm{Sch}_p^2\frac{y_A}{(y_A-y)^3}\left(\frac{\partial y}{\partial\bar{x}}\right)^2-6\sin\theta\cos\theta\left(\cos^2\theta-\frac{1}{3}\right)\times\mathrm{Sch}_p\sqrt{y_Ay_B}\frac{1-y_A}{(y-y_A)^3}\frac{\partial y}{\partial\bar{x}}\right]\frac{\partial y}{\partial\bar{x}}+\left(\cos^2\theta-\frac{1}{3}\right)\left((-2\cos^2\theta+\sin^2\theta)\mathrm{Sch}_py-3\sin\theta\times\cos\theta\mathrm{Sch}_p\sqrt{y_Ay_B}\frac{1-y}{y-y_A}-9\left(\cos^2\theta-\frac{1}{3}\right)\sin^2\theta\cos^2\theta\mathrm{Sch}_p^2\frac{y}{y_A-y}\frac{\partial y}{\partial\bar{x}}\right)\frac{\partial y}{\partial\bar{x}}=\frac{1}{2}[y^2-1+y_Ay_B\left(\frac{1-y}{y-y_A}\right)^2+9\sin^2\theta\cos^2\theta\left(\cos^2\theta-\frac{1}{3}\right)^2\mathrm{Sch}_p^2\left(\frac{y}{y_A-y}\right)^2\left(\frac{\partial y}{\partial\bar{x}}\right)^2-6\left(\cos^2\theta-\frac{1}{3}\right)\times\sin\theta\cos\theta\mathrm{Sch}_p\sqrt{y_Ay_B}y\frac{1-y}{(y-y_A)^2}\frac{\partial y}{\partial\bar{x}}\right]+y_B\frac{1-y}{y-y_A}+3\sin\theta\cos\theta\mathrm{Sch}_p\left(\cos^2\theta-\frac{1}{3}\right)\frac{\sqrt{y_Ay_B}}{y_A-y}\frac{\partial y}{\partial\bar{x}}+\frac{y^{1-\gamma_g}-1}{M_{s1}^2(\gamma_g-1)}+\frac{\gamma_p}{\gamma_p-1}y\left(1-y+\frac{1-y^{-\gamma_g}}{\gamma_gM_{s1}^2}\right)+\frac{y_B}{2}\left[1-\left(\frac{1-y_A}{y-y_A}\right)^2-9\sin^2\theta\cos^2\theta\left(\cos^2\theta-\frac{1}{3}\right)^2\times\mathrm{Sch}_p^2\frac{y_A}{y_B(y_A-y)^2}\left(\frac{\partial y}{\partial\bar{x}}\right)^2+6\sin\theta\cos\theta\mathrm{Sch}_p\left(\cos^2\theta-\frac{1}{3}\right)\frac{1-y_A}{(y-y_A)^2}\frac{y_A}{y_B}\frac{\partial y}{\partial\bar{x}}\right]-(-2\cos^2\theta+\sin^2\theta)\mathrm{Sch}_p\left(\cos^2\theta-\frac{1}{3}\right)\frac{\partial y}{\partial\bar{x}}\Bigg)-\frac{\gamma_p}{\gamma_gM_{s1}^2(\gamma_p-1)}\frac{P_{p1}}{P_{g1}}(1-y), \tag{28}$$

where $M_{s1}^2=\rho_1U_{x1}^2/\gamma_gP_{g1}=U_{x1}^2/a_{g1}^2$ is the thermal gas Mach number far upstream and a_g is the thermal gas sound speed. Here, $\bar{k}$ is the perpendicular diffusion coefficient normalized to the parallel diffusion coefficient ($=K_\perp/K_\parallel$).

Equation (28) is the general shock structure equation in the presence of both PUI collisionless heat flux and collisionless viscosity. The structure of an oblique MHD shock in the absence of energetic particle viscosity was investigated by Webb (1983). If we let η_p tend to zero, we obtain the same equation derived by Webb (1983),

$$\frac{\partial y}{\partial\bar{x}}=\frac{3(\gamma_p-1)(y-y_A)N(y)}{D(y)}(1-y), \tag{29}$$

where

$$N(y)=\frac{1}{2}y_Ay_B(1-y)-\frac{1}{2}(y-y_A)^2(y+1)+\frac{1}{\gamma_g-1}(y-y_A)^2\frac{y^{1-\gamma_g}-1}{M_{s1}^2(1-y)}+\frac{\gamma_p}{\gamma_p-1}y(y-y_A)^2\frac{1-y^{-\gamma_g}}{\gamma_gM_{s1}^2(1-y)}-\frac{(y-y_A)^2\gamma_pP_{p1}}{M_{s1}^2\gamma_gP_{g1}(\gamma_p-1)}+\frac{\gamma_p}{\gamma_p-1}\times y(y-y_A)^2+y_B(y-y_A)-\frac{\gamma_p}{2(\gamma_p-1)}y_By(y+1-2y_A);$$

$$D(y)=(y-y_A)^3-\frac{y^{-\gamma_g-1}}{M_{s1}^2}(y-y_A)^3-y_B(1-y_A)^2. \tag{30}$$

Equation (29) has two solution regimes. The first regime corresponds to smooth transitions connecting an upstream state ($y=1$) and a downstream state ($y=y_\infty$) via a unique solution. Thus, the energetic particle heat flux alone is sufficient to smooth the shock transition. However, the second regime needs additional dissipation. The solution of Equation (29) in the second regime is a nonphysical double-valued solution, and a smooth transition from upstream to downstream is impossible. As discussed by Whitham (1974), this case has a sonic point $y=y_s$ (i.e., the flow speed is equal to the thermal sound speed) greater than y_∞. Drury & Völk (1981), Axford et al. (1982), and Webb (1983) showed that it is necessary to insert a "gas subshock" in the flow to reach the downstream state. The assumption underlying the insertion of a gas subshock is that energetic particle dissipation is not sufficient to smooth the shock transition, and another dissipation mechanism due to the thermal gas must be provided. However, the assumption of adding thermal gas dissipation may not always be correct especially in the outer heliosphere, which is dominated by PUI or energetic particle pressure (McComas et al. 2017). Thus, PUIs may play a critical role in the dissipation process at interplanetary shocks propagating in the outer heliosphere, and adding a gas subshock may not be a reasonable assumption. As was predicted by Zank et al. (1996) and confirmed by Richardson et al. (2008), the dissipation mechanism at the HTS is provided primarily by reflected PUIs and not by thermal gas protons (see also Oka et al. 2011; Yang et al. 2015; Mostafavi et al. 2017b; Lembège & Yang 2018). The reflected

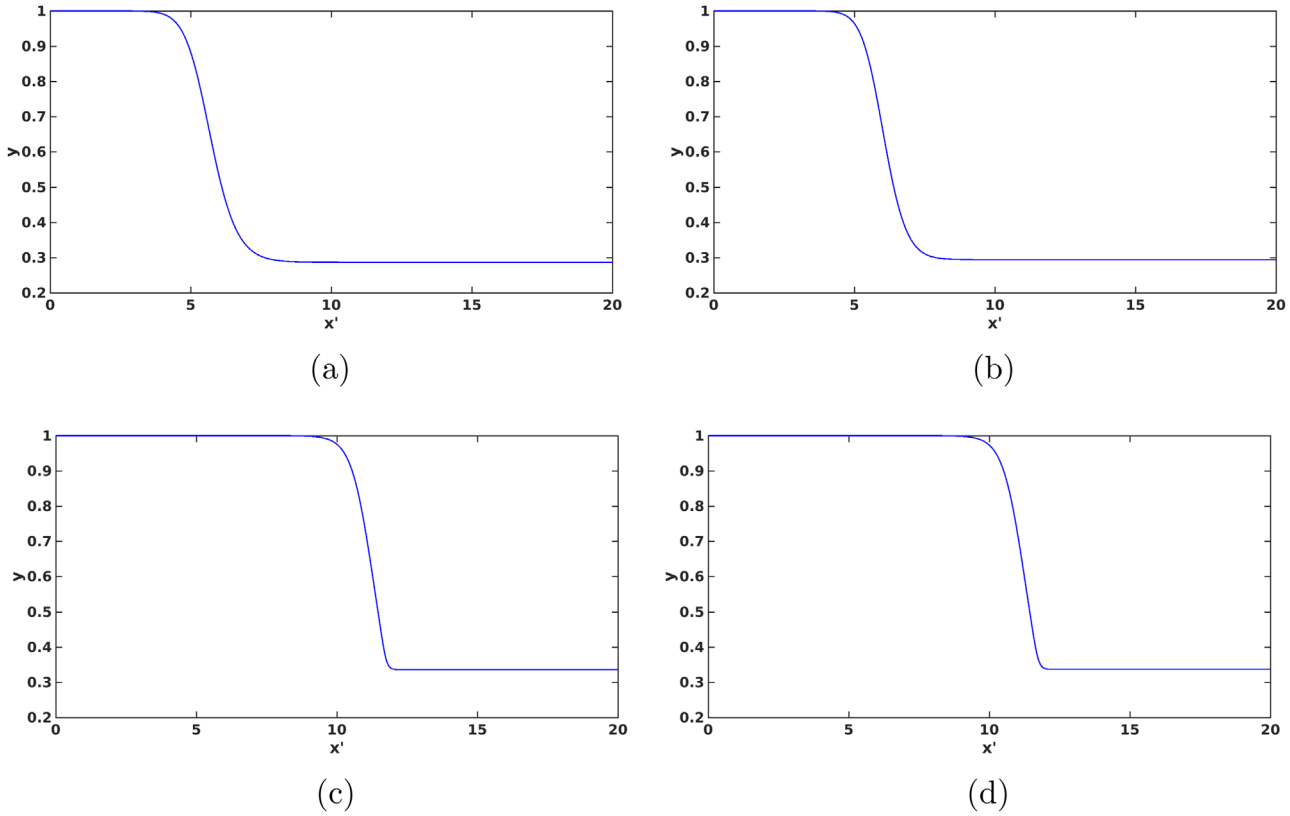

Figure 1. Smoothed shock transitions when both PUI collisionless viscosity and heat conduction are present. Here, $\gamma_g = \gamma_p = 5/3$, $P_{p1}/P_{g1} = 10.0$, $M_{s1} = 15$, and $M_{A1} = (y_A + y_B)^{-1/2} = 4.47$. The inverse compression ratio is plotted as a function of normalized distance for (a) $\theta = 0°$, i.e., a parallel shock. (b) $\theta = 17.5$. (c) $\theta = 80°$. (d) $\theta = 90°$, i.e., a perpendicular shock.

solar wind protons play a small dynamical role at the HTS and experience little heating. Consequently, the basic dissipation process at the HTS is due to the nearly isotropic PUIs. *Voyager 2* observations showed that the IHS is thermally dominated by energetic particles such as PUIs and ACRs, and the plasma beta is therefore $\beta = (P_g + P_p)/P_B \gg 1$ (Decker et al. 2015; Zank 2017 calculated $\beta \sim 14$). Shock waves propagating in the IHS may be largely dissipated by PUIs rather than thermal gas. Therefore, the inclusion of PUI dissipation is more appropriate than introducing a gas subshock in the IHS.

All shocks in a non-magnetized cold thermal gas have a smooth structure when energetic particles are included (Axford et al. 1982). However, Webb (1983) found that the structure of an MHD shock accelerating energetic particles with a cold gas upstream is not necessarily smoothed by heat conduction associated with energetic particles in some Mach number regimes. Webb (1983) concluded that a gas subshock is sometimes necessary in the absence of additional dissipation mechanisms, even in a cold thermal gas plasma.

Mostafavi et al. (2017a, 2017b) studied the structure of hydrodynamic shock waves (the case of very large plasma beta) in the presence of both PUI collisionless viscosity and collisionless heat flux terms. Since there is no change in magnetic field magnitude and direction across a parallel shock, the hydrodynamic shock structure model is similar to that of the parallel shock (i.e., $\theta = 0$, $y_B = 0$; the magnetic field is parallel to the shock normal). If we set $\theta = 0$ in our general Equation (28), we obtain the same shock structure equation as Mostafavi et al. (2017b),

$$\frac{d^2y}{d\bar{x}^2} + \frac{1}{Sc_p}\left[\frac{3}{4}\left(\left(\frac{y_s}{y}\right)^{\gamma_g+1} - 1\right) - 3Sc_p y\right] \times \frac{dy}{d\bar{x}} = \frac{1}{Sc_p}\frac{9}{4}\frac{\gamma_p}{\gamma_g M_{s1}^2}(1-y)P(y), \tag{31}$$

where

$$P(y) \equiv \gamma_g M_{s1}^2 \frac{\gamma_p + 1}{2\gamma_p}(y - \mu_p^2) - \left(1 + \frac{P_{p1}}{P_{g1}} - \frac{(\gamma_g - \gamma_p)}{\gamma_p(\gamma_g - 1)}\frac{(1 - y^{1-\gamma_g})}{(1-y)}\right), \tag{32}$$

$\mu_p^2 \equiv \frac{(\gamma_p - 1)}{(\gamma_p + 1)}$, and $y_s^{\gamma_g+1} \equiv \frac{1}{M_{s1}^2}$. Equation (31) is a second-order differential equation which has no singular point to introduce double-valued solutions. Mostafavi et al. (2017b) showed that the combination of both PUI collisonless heat flux and viscosity is sufficient to smooth all energetic particle mediated shocks in the absence of a magnetic field.

The structure of a perpendicular shock, i.e., for a magnetic field is perpendicular to the shock normal, can be obtained by

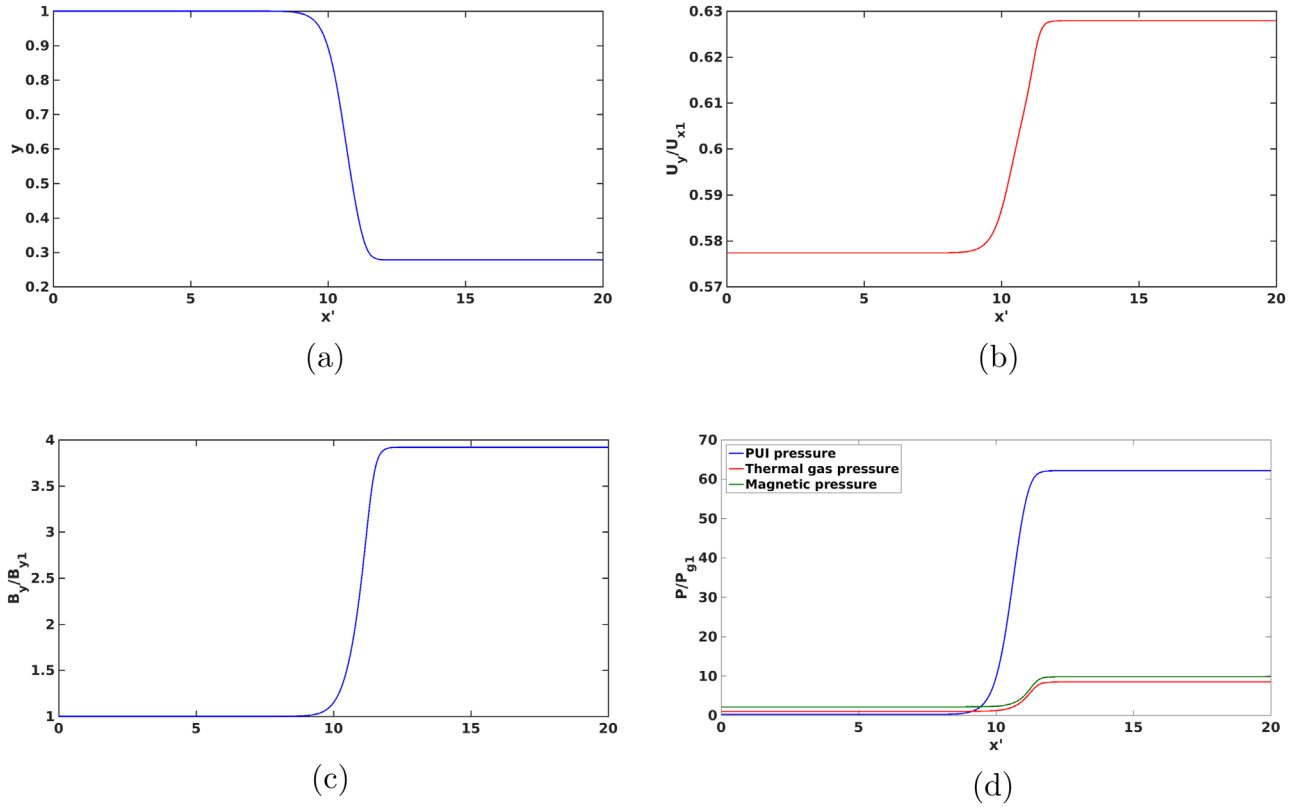

Figure 2. Smoothed shock transitions when both PUI viscosity and heat conduction are included. Here $\theta = 30°$, $\gamma_g = \gamma_p = 5/3$, $P_{p1}/P_{g1} = 0.2$, $M_{s1} = 8.0$, and $M_{A1} = (y_A + y_B)^{-1/2} = 5.0$. (a) Inverse compression ratio, U_x/U_{x1}, showing the smoothed shock as a function of normalized position. (b) Tangential component of velocity as a function of normalized distance. (c) Tangential component of magnetic field as a function of normalized distance. (d) PUI, thermal gas, and magnetic field pressure normalized to the thermal gas pressure far upstream as a function of distance.

setting $\theta = \pi/2$ in Equation (28),

$$\frac{d^2y}{d\bar{x}^2} + \frac{3}{\mathrm{Sch}_p}\left[\left(\frac{1}{M_{s1}^2}\left(\frac{1}{y}\right)^{\gamma_p+1} - 1\right) - \mathrm{Sch}_p y + \frac{y_B}{y^3}\right] \times \frac{dy}{d\bar{x}} = \frac{9}{\mathrm{Sch}_p}\frac{\gamma_p}{\gamma_g M_{s1}^2}(1-y)V(y), \quad (33)$$

where

$$V(y) \equiv \gamma_g M_{s1}^2 \frac{\gamma_p + 1}{2}\left(y - \frac{\gamma_p - 1}{\gamma_p + 1}\right) - \left(1 + \frac{P_{p1}}{P_{g1}} - \frac{(\gamma_g - \gamma_p)}{\gamma_p(\gamma_g - 1)}\frac{(1 - y^{1-\gamma_g})}{(1-y)} - \gamma_g M_{s1}^2 \frac{y_B}{2y}\left(\frac{\gamma_p - 2}{\gamma_p} - y\right)\right). \quad (34)$$

This equation is structurally similar to that of the perpendicular VLISM shock wave studied by Mostafavi & Zank (2018). However, in the VLISM, the dissipation is provide by the thermal gas and not PUIs (Mostafavi & Zank 2018).

Solutions for four different shock obliquity angles for the PUI collisionless viscous-heat conduction, Equation (28), are shown in Figures 1(a)–(d). In the absence of collisionless viscosity, the parameters chosen for Figures 1(a)–(d) ensure that the solutions are double-valued, which means that heat conduction alone is insufficient to smooth the shock structure (Webb 1983). However, the inclusion of collisionless viscosity along with heat conduction leads to the complete smoothing of the shock transition from the upstream to the downstream state for all of these angles. The only angle at which the shock structure is not smooth is at an angle $\theta = 54.^{\circ}7$. This limitation is not physical but technical, since the assumed form of the viscosity term goes to zero at this specific angle (the root of $\cos^2\theta - 1/3 = 0$). This singular behavior can be eliminated by a more complete physical treatment of the viscosity term. For now, we do not consider this aspect of the problem. The thickness of shock waves is determined by the dominant dissipation mechanism of the system. Equation (17) shows that the viscosity term, Π_{xx}, for a parallel shock is larger than that of a perpendicular shock. Since the parallel diffusion coefficient is larger than the perpendicular diffusion coefficient ($K_\parallel > K_\perp$), the thickness of the parallel shock 1(a) is larger than that of the perpendicular shock 1(d).

Figure 2 shows an example of a shock wave for the case where $\theta = 30°$, $M_{s1} = 8.0$, $M_{A1} = 5.0$, and $P_{p1}/P_{g1} = 0.2$. Figures 2(a) and (b) are plots of the inverse compression ratio and the normalized tangential component of the velocity as a function of normalized distance, all of which show a smooth shock transition. The change in the tangential component of the magnetic field along the y-axis as a function of normalized position is plotted in Figure 2(c). Figure 2(d) shows normalized plots of the PUI, thermal gas, and magnetic pressure along the shock transition.

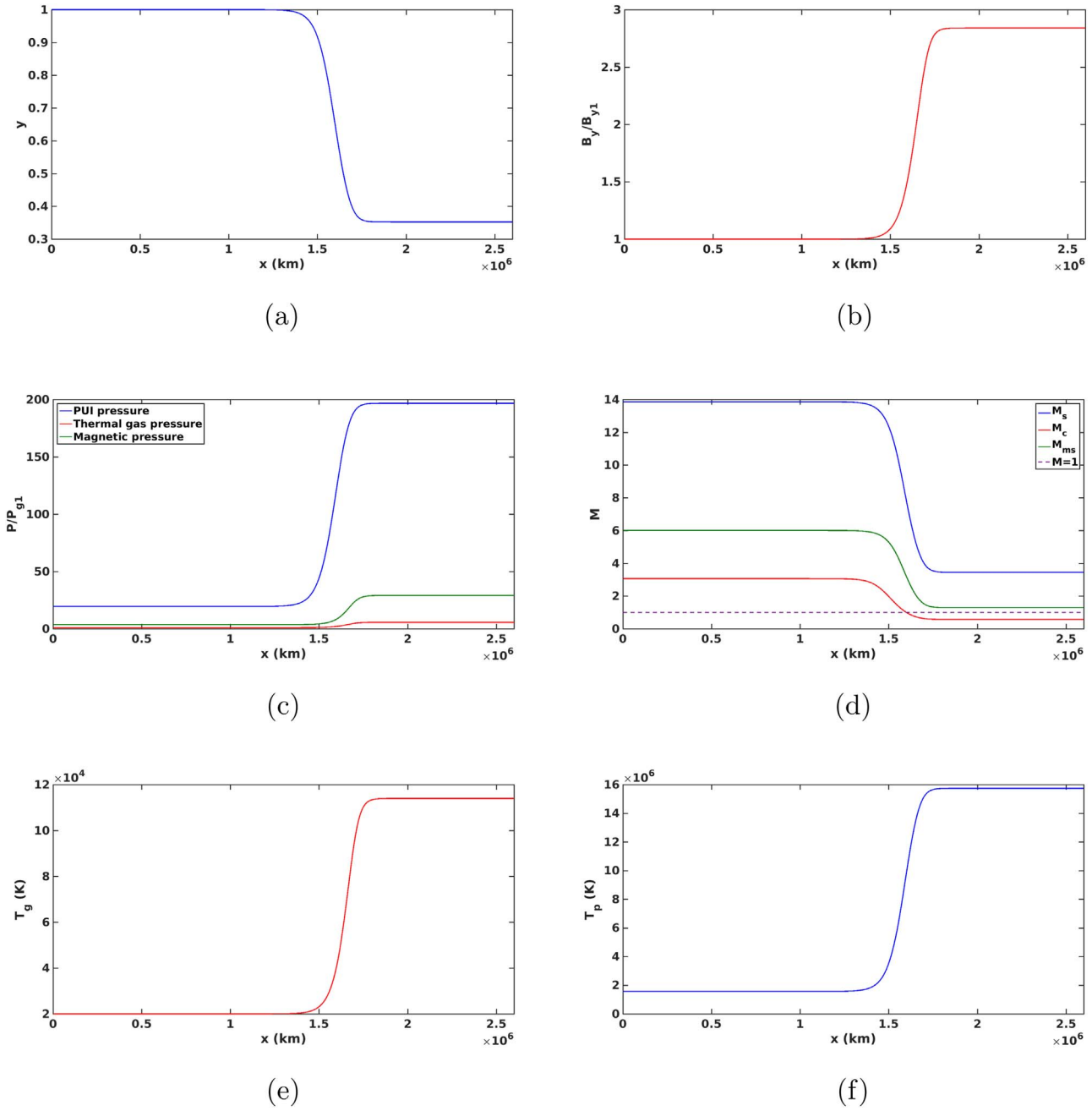

Figure 3. Smoothed shock transition corresponding to a perpendicular HTS when both the PUI heat flux and viscosity are included. Here, $\theta = 90°$, $\gamma_g = \gamma_p = 5/3$, $P_{p1}/P_{g1} = 19.5$, $M_{s1} = 13.85$, and $M_{A1} = (y_B)^{-1/2} = 6.6$. (a) Inverse compression ratio, U_x/U_{x1}, showing the smoothed shock as a function of unnormalized position. (b) The tangential component of the magnetic field normalized to the upstream value as a function of unnormalized distance. (c) PUI, thermal gas, and magnetic field pressure normalized to the thermal gas pressure far upstream. The HTS is mediated by PUIs with almost all of the upstream ram energy being converted to downstream PUI internal energy. (d) The thermal gas Mach number, $M_s \equiv u/a_g$, and the combined thermal gas, fast magnetosonic Mach number, $M_{ms} \equiv u\Big/\sqrt{a_g^2 + V_A^2}$, and PUI Mach number, $M_c \equiv u\Big/\sqrt{a_g^2 + a_p^2}$, through the HTS. Relative to the combined sound speed, the flow is subsonic downstream of the HTS. (e) The unnormalized thermal gas temperature through the HTS as a function of unnormalized distance shows that thermal gas remains relatively cold. (f) The unnormalized PUI temperature through the HTS as a function of unnormalized distance shows that PUIs are strongly heated at the HTS.

4. The Heliospheric Termination Shock

The physical properties of the supersonic solar wind charged particles change dramatically at the HTS, which is an example of a collisionless supercritical shock. *Voyager 2* observations showed that the temperature of thermal gas upstream of the HTS is about 20,000 K. The PUI temperature upstream of HTS was estimated to be 1.56×10^6 K by Zank et al. (2010) and Burrows et al. (2010). Even though the PUI number density is about 20% that of the total thermal protons, its pressure is the dominant thermal component and much greater than that of the thermal gas ($P_{p1} = 5.38 \times 10^{-15}$ Pa $\gg P_{g1} = 2.76 \times 10^{-16}$ Pa). The measurements taken by the *Voyager 2* crossing revealed that the HTS was unlike heliospheric shocks observed previously by other spacecraft (Richardson et al. 2008; Richardson 2008). Global MHD models predicted that the temperature downstream of the HTS should be $\sim 10^6$ K. However, the plasma instrument on *Voyager 2* measured a thermal plasma temperature of

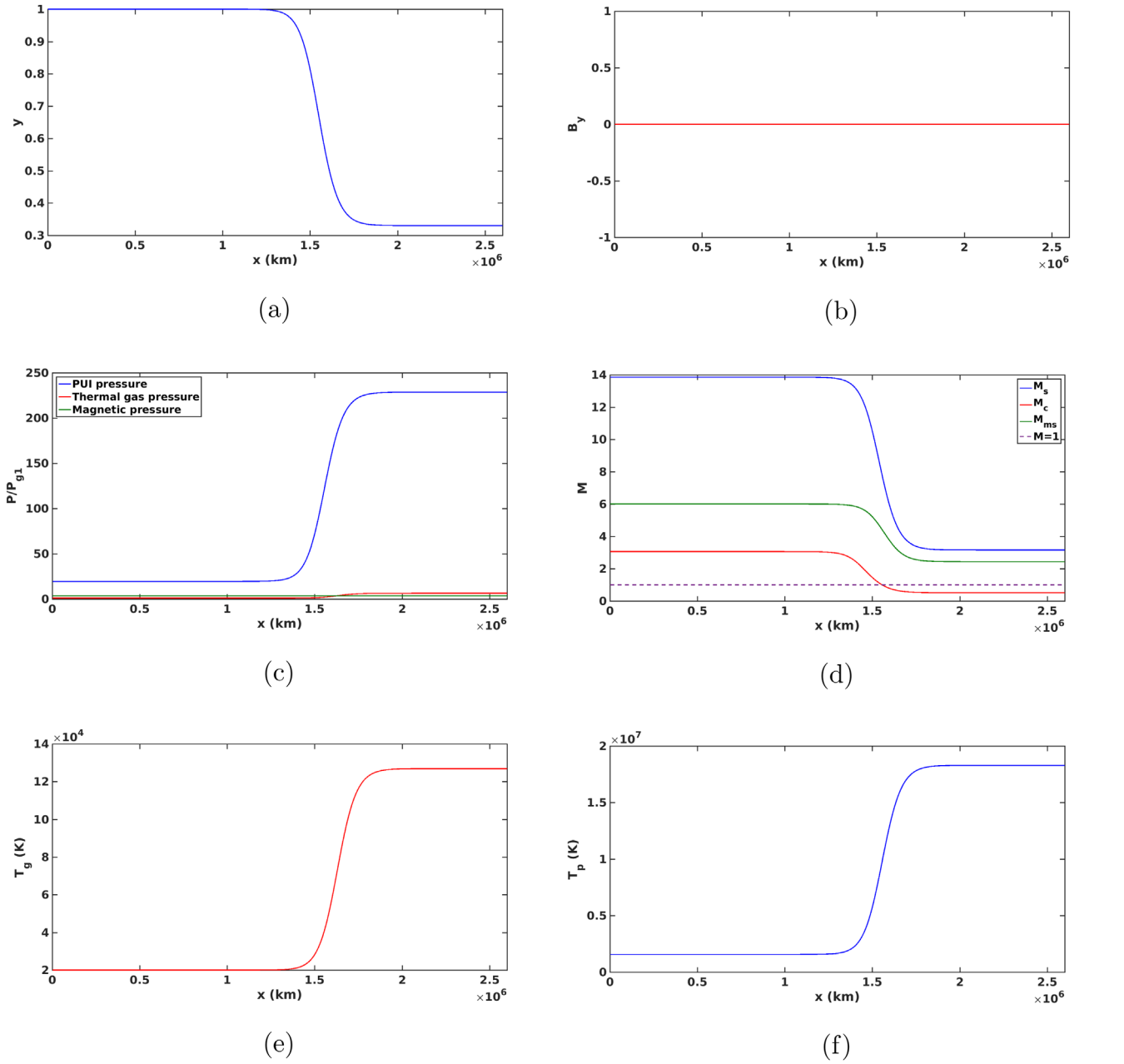

Figure 4. Smoothed shock transition corresponding to a parallel HTS when both the PUI heat flux and viscosity are included. Here, all of the parameters are the same as in Figure 3 except $\theta = 0°$ and $M_{A1} = (y_A)^{-1/2} = 6.6$. (a) Inverse compression ratio as a function of unnormalized position. (b) The tangential component of the magnetic field is zero for the parallel shock. (c) PUI, thermal gas, and magnetic field pressure normalized to the thermal gas pressure far upstream. (d) The thermal gas Mach number, $M_s \equiv u/a_g$, fast magnetosonic Mach number, $M_{ms} \equiv u\Big/\sqrt{a_g^2 + V_A^2}$, and the combined thermal gas and PUI Mach number, $M_c \equiv u\Big/\sqrt{a_g^2 + a_p^2}$, through the HTS. Relative to the combined sound speed, the flow is subsonic downstream of the HTS. (e) The unnormalized thermal gas temperature through the HTS as a function of unnormalized distance. (f) The unnormalized PUI temperature through the HTS as a function of unnormalized distance.

~120,000–180,000 K downstream of the HTS (Richardson 2008; Richardson et al. 2008). A very small percentage of the upstream solar wind flow energy is converted to downstream heating of the thermal gas. Most of the energy goes instead to heat non-thermalized PUIs. We use our model to numerically simulate the second crossing of the HTS, TS-2, by *Voyager 2* based on upstream parameters from the Richardson et al. (2008) observations. TS-2 moved with a speed of about 90 km s^{-1} with respect to the Sun in the outward direction.

It is generally believed that the HTS is nearly perpendicular because of its large distance from the Sun and the Parker spiral structure of the magnetic field. However, this is true in the absence of any turbulence and fluctuations on the shock surface. The creation of energetic PUIs and ACRs in the outer heliosphere and their acceleration at a shock leads to the generation of turbulence and instabilities that can affect the shock structure (Zank & McKenzie 1987; Zank 1999). Upstream density and magnetic field fluctuations can affect the shock structure and introduce rippling of the shock surface (Lu et al. 2009). The plasma instrument and magnetometer on *Voyager 2* detected at least five crossings of the HTS (Richardson et al. 2008). The multiple crossings of the HTS have been interpreted (Yang et al. 2015; Lembège & Yang 2018) as possibly due to a rippled or reforming shock, and it is

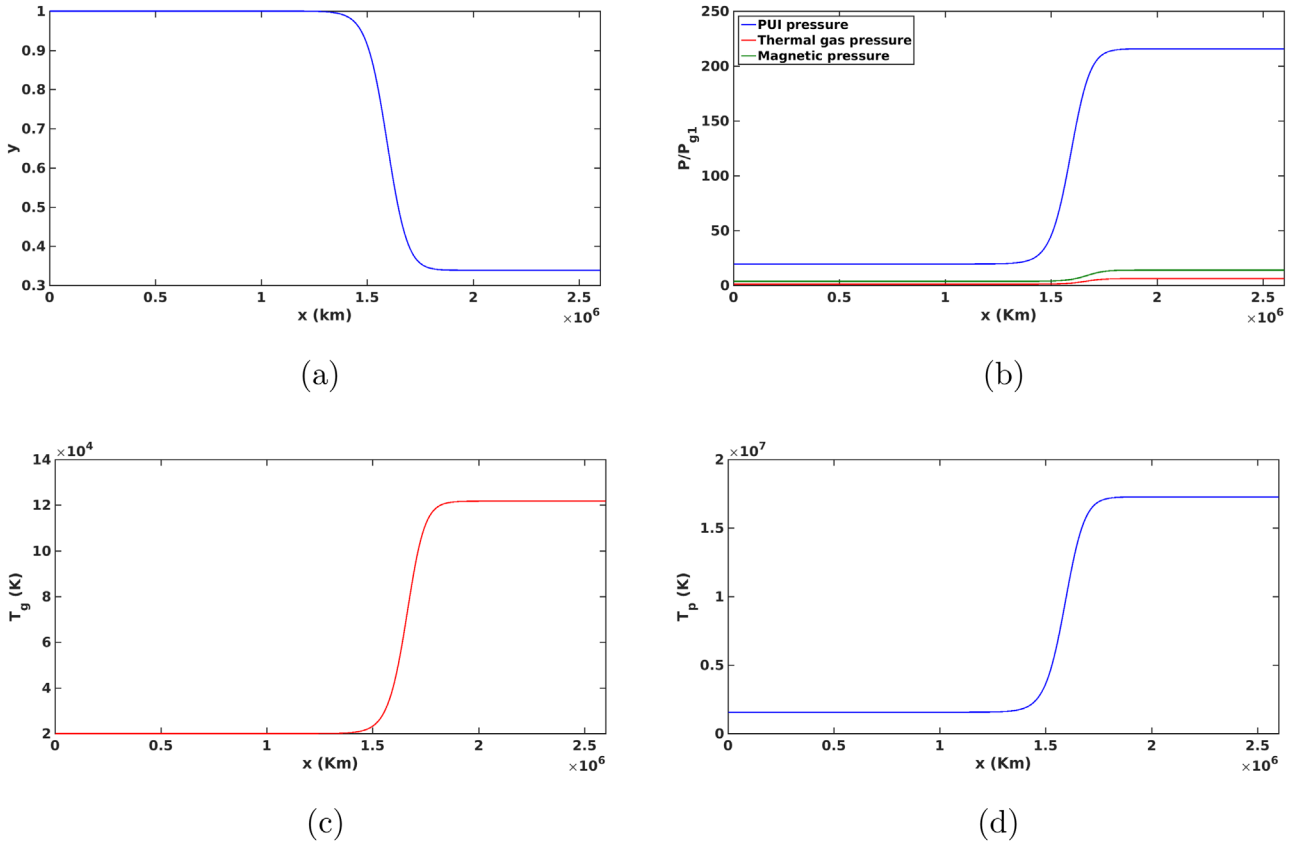

Figure 5. Smoothed shock transition corresponding to an oblique HTS when both the PUI heat flux and viscosity are included. Here, all of the parameters are the same as in Figures 3–4 except $\theta = 30°$. (a) Inverse compression ratio as a function of normalized position. (b) PUI, thermal gas, and magnetic field pressure normalized to the thermal gas pressure far upstream. (c) The unnormalized thermal gas temperature through the HTS as a function of unnormalized distance. (d) The unnormalized PUI temperature through the HTS as a function of unnormalized distance.

Table 1
The Downstream Parameters for Either a Perpendicular HTS or Parallel HTS

Parameters	Downstream of the Perpendicular HTS	Downstream of the Parallel HTS
Compression ratio	2.83	3
Thermal gas temperature (K)	1.13×10^5	1.26×10^5
PUI temperature (K)	1.57×10^7	1.82×10^7
Thermal gas pressure (kg m^{-1} s^{-2})	1.57×10^{-15}	1.75×10^{-15}
PUI pressure (kg m^{-1} s^{-2})	5.42×10^{-14}	6.3×10^{-14}
Magnetic pressure (kg m^{-1} s^{-2})	8.02×10^{-15}	9.94×10^{-16}

possible that the HTS is, in some regions, an oblique shock or even a parallel shock. TSPs, which are believed to be PUIs that are energized and accelerated at the HTS, can be reflected into the heliosphere along the magnetic field at an oblique or quasi-parallel HTS. *Voyager 1* observations of TSPs showed a significant increase in the number density a few months before the HTS crossing (Cummings et al. 2003; McDonald et al. 2003). The distance that these energetic particles reached is much greater than the particles' gyroradius. It is therefore possible that the TSPs propagated along the magnetic field from the HTS as a result of reflection at a quasi-parallel HTS (Florinski et al. 2008).

Figures 3 and 4 show the properties of a perpendicular and parallel HTS, respectively using the same upstream conditions. Figure 3(a) shows that the compression ratio of the perpendicular HTS, $r = 1/y$, is about 2.83, whereas *Voyager 2* observations showed a compression ratio of about 2.38 ± 0.4 for a nearly perpendicular shock (Burlaga et al. 2008). In contrast, the parallel HTS yields a larger compression ratio of about 3 (Figure 4(a)). The normalized tangential component of the magnetic field as a function of unnormalized distance is shown in Figures 3(b) and 4(b). The normal component of the magnetic field, B_x, is zero for the perpendicular case. As usual, the downstream density and tangential magnetic field components at a perpendicular shock increase by the same fraction as the normal velocity decreases (i.e., $B/\rho=$ constant; Zank et al. 2006). However, at the parallel shock, the magnitude and direction of the magnetic field do not change across the shock, and the shock, therefore, becomes a purely gas-dynamic shock (Figure 4(b)). Figures 3(c) and 4(c) show plots of the normalized PUI, thermal gas, and magnetic field pressure as a function of unnormalized position. The thermal gas experiences adiabatic heating only, and the incident ram pressure is converted primarily to PUI and magnetic pressure (almost all being converted to PUI pressure). The PUI and thermal gas pressure at the downstream of the parallel HTS are greater than those at the perpendicular HTS. The thermal gas Mach number through the HTS (Figures 3(d) and 4(d))

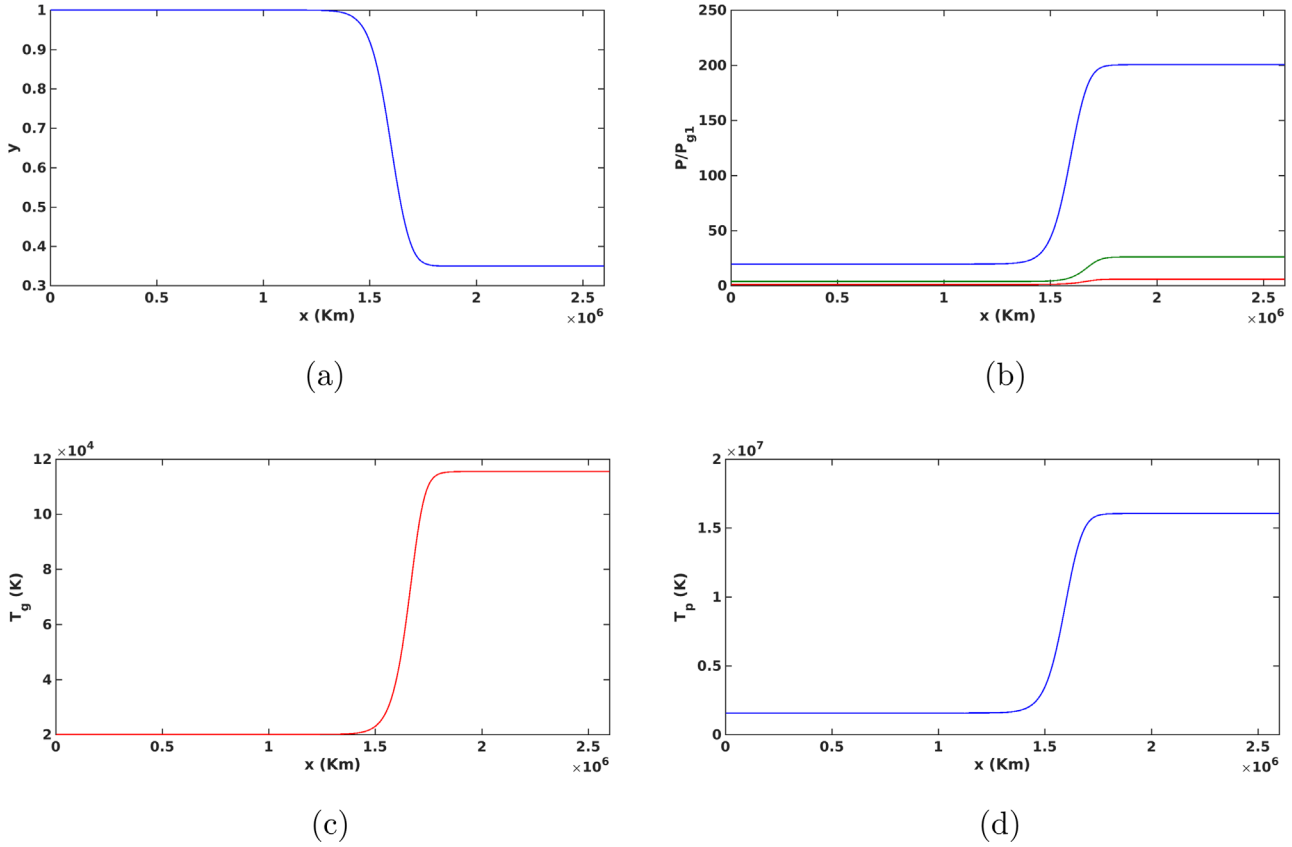

Figure 6. Smoothed shock transition corresponding to an oblique HTS when both the PUI heat flux and viscosity are included. Here, all of the parameters are the same as in Figures 3–5 except $\theta = 75°$. (a) Inverse compression ratio as a function of normalized position. (b) PUI, thermal gas, and magnetic field pressure normalized to the thermal gas pressure far upstream. (c) The unnormalized thermal gas temperature through the HTS as a function of unnormalized distance. (d) The unnormalized PUI temperature through the HTS as a function of unnormalized distance.

shows that the flow with respect to the thermal gas downstream of the shock remains supersonic. This is consistent with the *Voyager 2* observations (Richardson et al. 2008) that showed that the small increase in thermal gas temperature across the shock did not change the flow from supersonic upstream to subsonic downstream. The change of fast magnetosonic Mach number through the HTS shows that the magnetic field and thermal gas pressure are not sufficient to ensure a supersonic–subsonic transition. However, the combined PUI and thermal gas Mach number through the HTS shows that the inclusion of PUIs changes the flow from supersonic to subsonic. This illustrates that PUIs provide the dominant dissipation mechanism at the HTS. Figures 3(e)–(f) and 4(e)–(f) show unnormalized plots of the thermal gas and PUI temperature profiles as a function of unnormalized distance. PUIs and thermal gas are more heated downstream of the parallel HTS than at the perpendicular HTS. The plasma beta downstream of the HTS, in the IHS, is about 0.2 (<1). However, with the inclusion of PUIs, the plasma beta is about 7, which is consistent with *Voyager 2* observations (Decker et al. 2015).

Comparisons between the parallel HTS and perpendicular HTS are listed in Table 1. As discussed, the parallel HTS is more compressed. The PUI and thermal gas pressure are larger at the parallel shock than at the perpendicular shock, suggesting that important differences can arise from the obliquity of a shock wave. In view of these results, we conclude this section by showing results for a quasi-parallel ($\theta = 30°$) and quasi-perpendicular ($\theta = 75°$) HTS. The results are shown in Figures (5) and (6).

5. Conclusions

Energetic particles such as PUIs, ACRs, and SEPs play a critical role in determining the structure of heliospheric shock waves. In this work, we distinguish energetic particles from thermal solar wind particles and thus distinguish the dissipation mechanisms responsible for determining the structure of shocks in the heliosphere. We derived a general collisionless oblique magnetized shock wave structure equation, which includes both the energetic particle collisionless heat conduction and viscosity. The second-order shock structure equation shows that all transitions from the upstream to the downstream state are smooth except for the angle at which the PUI viscosity goes to zero ($\theta = 54.^{\circ}7$). This limitation does not have a physical meaning, and is due to our assumption of a slightly simplified form of the viscosity coefficient.

We showed that the region downstream of the HTS is supersonic with respect to the thermal solar wind plasma, but subsonic when PUIs are included self-consistently. Thus, most of the upstream solar wind flow energy is converted to downstream PUI heating and the thermal solar wind remains relatively cold. The structure of shock waves in the outer heliosphere can be affected by turbulence and instabilities because of the existence of PUIs and ACRs. These fluctuations can introduce rippling on the shock surface in the outer heliosphere. The HTS is therefore not always a quasi-perpendicular shock and in some regions can be an oblique or a parallel shock. The TSPs that propagate along the interplanetary magnetic field from the HTS to distances much

greater than the particle's gyroradius can result from reflection at regimes where the HTS is a quasi-parallel. We studied the oblique, parallel, and perpendicular HTS. On comparing the properties of a parallel and perpendicular HTS, we find that the parallel HTS has a larger compression ratio and thus heats the PUIs and thermal gas more than at a perpendicular HTS. The parallel HTS is thicker than the perpendicular HTS because of the correspondingly smaller heat flux across the magnetic field than along it.

P.M. acknowledges the support of a NASA Earth and Space Science Fellowship Program-Grant 16-HELIO16F-0022. G.P.Z. acknowledges the support of NASA grants NNX14AC08G, NNX15AI65G, NNX17AB04G, NNX14AJ53G, and the NSF EPSCoR RII-Track-1 Cooperative Agreement OIA-1655280. G.M.W. acknowledges partial support by grant NNX15A165G.

ORCID iDs

P. Mostafavi https://orcid.org/0000-0002-3808-3580
G. P. Zank https://orcid.org/0000-0002-4642-6192
G. M. Webb https://orcid.org/0000-0002-0617-9502

References

Axford, W. I., Leer, E., & McKenzie, J. F. 1982, A&A, 111, 317
Burgess, D., & Scholer, M. 2007, PhPl, 14, 012108
Burlaga, L. F., Ness, N. F., Acuña, M. H., et al. 2008, Natur, 454, 75
Burlaga, L. F., Ness, N. F., Gurnett, D. A., & Kurth, W. S. 2013, ApJL, 778, L3
Burrows, R. H., Zank, G. P., Webb, G. M., Burlaga, L. F., & Ness, N. F. 2010, ApJ, 715, 1109
Coroniti, F. V. 1970, JPlPh, 4, 265
Cummings, A. C., Stone, E. C., Burlaga, L. F., et al. 2003, Proc. ICRC, 7, 3777
Decker, R. B., Krimigis, S. M., Roelof, E. C., & Hill, M. E. 2015, JPhCS, 577, 012006
Drury, L. O., & Völk, J. H. 1981, ApJ, 248, 344
Earl, J. A., Jokipii, J. R., & Morfill, G. 1988, ApJL, 331, L91
Fisk, L. A., Kozlovsky, B., & Ramaty, R. 1974, ApJL, 190, L35
Florinski, V., Decker, R. B., le Roux, J. A., & Zank, G. P. 2009, GeoRL, 36, L12101
Florinski, V., Zank, G. P., & Le Roux, J. A. 2008, AdSpR, 41, 361
Jokipii, J. R., & Williams, L. L. 1992, ApJ, 394, 184
Kennel, C. F., Edmiston, J. P., & Hada, T. 1985, GMS, 34, 1
Lario, D., Decker, R. B., Roelof, E. C., & Viñas, A.-F. 2015a, ApJ, 813, 85
Lario, D., Decker, R. B., Roelof, E. C., & Viñas, A.-F. 2015b, JPhCS, 642, 012014
Lembège, B., & Yang, Z. 2018, ApJ, 860, 84
Lu, Q., Hu, Q., & Zank, G. P. 2009, ApJ, 706, 687
Marshall, W. 1955, RSPSA, 233, 367
McComas, D., Allegrini, F., Bagenal, F., et al. 2008, SSRv, 140, 261
McComas, D. J., Alexashov, D., Bzowski, M., et al. 2012, Sci, 336, 1291
McComas, D. J., Zirnstein, E. J., Bzowski, M., et al. 2017, ApJS, 233, 8
McDonald, F. B., Stone, E. C., Cummings, A. C., et al. 2003, Natur, 426, 48
Mostafavi, P., & Zank, G. P. 2018, ApJL, 854, L15
Mostafavi, P., Zank, G. P., & Webb, G. M. 2017a, JPhCS, 900, 012016
Mostafavi, P., Zank, G. P., & Webb, G. M. 2017b, ApJ, 841, 4
Oka, M., Zank, G. P., Burrows, R. H., & Shinohara, I. 2011, in AIP Conf. Ser., Vol. 1366, Partially Ionized Plasmas Throughout The Cosmos, ed. V. Florinski et al. (Melville, NY: AIP), 53
Richardson, J. D. 2008, GeoRL, 35, 23104
Richardson, J. D., Kasper, J. C., Wang, C., Belcher, J. W., & Lazarus, A. J. 2008, Natur, 454, 63
Riley, P., Caplan, R., Giacalone, J., Lario, D., & Liu, Y. 2016, ApJ, 819, 57
Russell, C. T., Mewaldt, R. A., Luhmann, J. G., et al. 2013, ApJ, 770, 38
Sagdeev, R. Z. 1979, RvMP, 51, 11
Stone, E. C., Cummings, A. C., McDonald, F. B., et al. 2005, Proc. ICRC, 2, 43
Webb, G. M. 1983, A&A, 127, 97
Webb, G. M. 1989, ApJ, 340, 1112
Webb, G. M., Drury, L. O., & Volk, H. J. 1986, A&A, 160, 335
Whitham, G. B. 1974, Linear and Nonlinear Waves, Vol. 1 (New York: Wiley)
Yang, Z., Liu, Y. D., Richardson, J. D., et al. 2015, ApJ, 809, 28
Ye, J., le Roux, J. A., & Arthur, A. D. 2016, ApJ, 826, 117
Zank, G. P. 1999, SSRv, 89, 413
Zank, G. P. 2015, ARA&A, 53, 449
Zank, G. P. 2016, GSL, 3, 22
Zank, G. P., Du, S., & Hunana, P. 2017, ApJ, 842, 114
Zank, G. P., Heerikhuisen, J., Pogorelov, N. V., Burrows, R., & McComas, D. 2010, ApJ, 708, 1092
Zank, G. P., Heerikhuisen, J., Wood, B. E., et al. 2013, ApJ, 763, 20
Zank, G. P., Hunana, P., Mostafavi, P., & Goldstein, M. L. 2014, ApJ, 797, 87
Zank, G. P., & McKenzie, J. F. 1987, JPlPh, 37, 347
Zank, G. P., Mostafavi, P., & Hunana, P. 2016, JPhCS, 719, 012014
Zank, G. P., Pauls, H. L., Cairns, I. H., & Webb, G. M. 1996, JGR, 101, 457
Zank, G. P., Shaikh, D., & Ao, X. 2006, in AIP Conf. Ser. 858, Physics of the Inner Heliosheath, ed. J. Heerikhuisen et al. (Melville, NY: AIP), 308
Zirnstein, E. J., Heerikhuisen, J., Zank, G. P., et al. 2014, ApJ, 783, 129